ELSEVIER Materials and Design 59 (2014) page: 516–523

http://dx.doi.org/10.1016/j.matdes.2014.03.012

A study of manufacturing tubes with nano/ultrafine grain structure by stagger spinning

Qinxiang Xia [a]*, Gangfeng Xiao[a], Hui Long [b], Xiuquan Cheng [c], Baojian Yang [a]

[a] School of Mechanical & Automotive Engineering, South China University of Technology, China

[b] Department of Mechanical Engineering, The University of Sheffield, UK

[c] Department of Aircraft Maintenance Engineering, Guangzhou Civil Aviation College, China

* Corresponding author: E-mail address: meqxxia@scut.edu.cn

Abstract

A new method of manufacturing tubes with nano/ultrafine grain structure by stagger spinning and recrystallization annealing is proposed in this study. Two methods of the stagger spinning process are developed, the corresponding macro forming quality, microstructural evolution and mechanical properties of the spun tubes made of ASTM 1020 steel are analysed. The results reveal that a good surface smoothness and an improved spin-formability of spun parts can be obtained by the process combining of 3-pass spinning followed by a 580 ºC× 0.5 h static recrystallization and 2-pass spinning with a 580 ºC×1 h static recrystallization annealing under the severe thinning ratio of wall thickness reduction. The ferritic grains with an average initial size of 50 μm are refined to 500 nm after stagger spinning under the 87% thinning ratio of wall thickness reduction. The equiaxial ferritic grains with an average size of 600 nm are generated through re-nucleation and grain growth by subsequent recrystallization annealing at 580 ºC for 1-hour heat preservation. The tensile strength of spun tubes has been founded to be proportional to the reciprocal of Layer Spacing of Pearlite (LSP), and the elongation is inversely proportional to the reciprocal of LSP. This study shows that the developed method of stagger power spinning has the potential to be used to manufacture bulk metal components with nano/ultrafine grain structure.

Keywords: Stagger spinning, Nano/ultrafine crystal, Tube, Recrystallization annealing

1. Introduction

Materials with nano/ultrafine grain structures are widely used in engineering applications due to their high strength and ductility, good surface smoothness, refined microstructure and super-plasticity at room temperature, as reported by Terry et al. [1]. Development of metal forming processes to achieve severe plastic deformation (SPD) has become one of recent research focuses in manufacturing metal components with nano/ultrafine grains to achieve refined microstructure, unique crystallographic texture and superior mechanical properties. Material processing using metal forming processes is considered as one of the most effective methods to manufacture bulk metal components with nano/ultrafine grained structures. A considerable number of SPD methods have been proposed and developed in recent years. These included ECAP (Equal Channel Angular Pressing), HPT (High Pressure Torsion), ARB (Accumulative Roll Bonding), and MSF (Multiple Stage Forging) as reported by Valiev [2]. Stoica [3] reported that the ECAP method was used to obtain ultrafine-grained Mg alloys which achieved better thermo-mechanical properties. Jiang et al. [4] studied the effects of increasing degree of HPT deformation and subsequent annealing on the evolution of microstructure and microhardness of copper alloy. Salimi et al. [5] adopted the ARB method to manufacture a carbon nanotube (CNT). Yang et al. [6] proposed a MSF method to achieve a large cumulative strain of 4.8 for manufacturing components of fine-grained magnesium alloy AZ31.

Metal spinning processes belong to the near net-shape forming technology. During spinning, a continuous and localized plastic deformation occurs in the metal blank to form an axis-symmetrical hollow part by means of the roller feeding movement and rotational motion of the mandrel, as outlined by Wang and Long [7]. Power spinning, which involves spinning with wall thickness thinning, consists of shear spinning to manufacture conically tubes and flow forming to manufacture tubes, as summarised by Wong et al. [8] and Xia et al. [9]. The recent research to manufacture tubes using power spinning has been mainly focused on the investigation of effects of process parameters on forming quality, mechanical properties and dimension accuracy. Hamid R. et al. [10] experimentally investigated the effects of thickness reduction on the mechanical properties and spinning accuracy of tubes of 7075-O aluminium. The experimental results showed that with the increase of thickness reduction, the yield strength, ultimate strength, surface hardness, and grain refining were all increased. On the other hand, it had adverse effect on geometrical accuracy, i.e.,

diametrical dimension, surface smoothness, and elongation of spun tubes. Xu et al. [11] studied the microstructure evolution and mechanical properties of TA15 alloy tubes during hot spinning. The results showed that with the increase of spinning passes, the fiber microstructure took shape gradually in axial direction, and the circumferential microstructure was also stretched visibly along the circumferential direction. As a result, the tensile strength was increased and elongation was decreased in both axial and circumferential directions.

There is no literature found referring to the study of manufacturing nano/ultrafine grain structures for bulk metal components by spinning processes. To explore the possibility of manufacturing components with nano/ultrafine grain structures by power spinning, two methods of stagger spinning processes are developed and experimentally tested in this study. The spinning process design, microstructural evolution during spinning and effects of microstructure on the mechanical properties of spun tubes are analysed.

2. Experimental design

2.1 Selection of spinning method

Stagger spinning is a type of power spinning processes to manufacture thin walled and hollow tubes. Typically, two or more rollers (usually three rollers) are used, and there is a certain distance between rollers along both axial and radial directions, as reported by Xia et al. [12]. To simplify the illustration of stagger spinning process, three rollers are positioned on the same longitudinal cross-section, as shown in Fig. 1. By using three-roller stagger spinning, the thinning ratio of one pass is divided among three rollers. The process is superior to three passes spinning processes by using single roller because in the stagger spinning not only the radial spinning force is equilibrated by the three rollers, but also the deformation area is in the state of three-dimensional compressive stresses. By developing a balanced design of each stagger distance between every two rollers, the degree of material deformation and geometrical accuracy of the spun part can be improved, as reported by Cheng et al. [13].

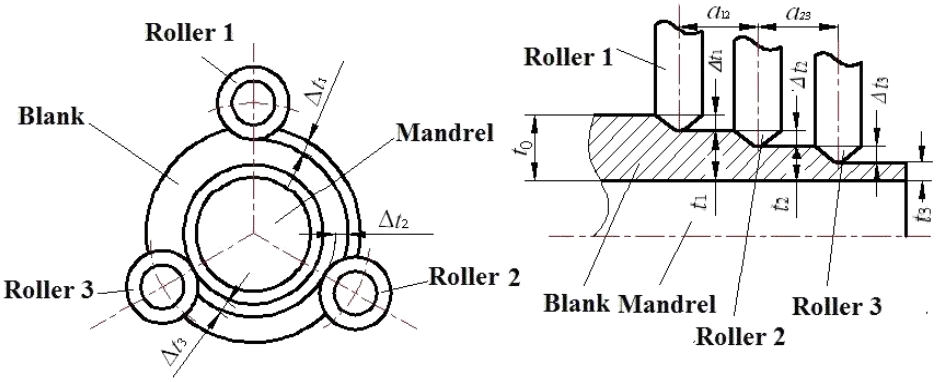

Fig.1. Illustration of stagger power spinning.

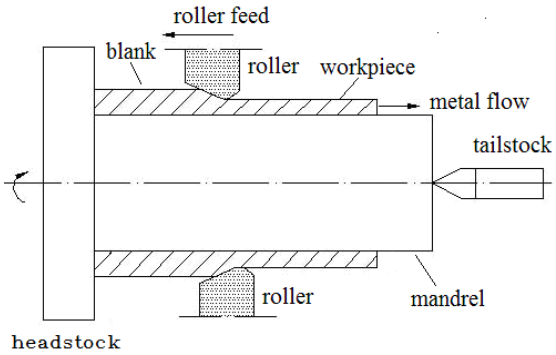

Fig.2. Illustration of backward power spinning.

For the manufacturing of the tubes, backward power spinning process is generally used, as shown in Fig.2. The deformed material in the contact zones is in a three-dimensionally compressive stress state, which contributes to the plasticity of the materials and beneficial to the refinement of grains. Therefore, the three-roller backward stagger spinning method is adopted in this study to manufacture tubes with nano/ultrafine grain structure.

2.2 Determination of process parameters

The macro forming quality and microstructure of spun part is directly influenced by the spinning process parameters. For three-roller stagger spinning, main process parameters influencing the macro forming quality and micro organization structure are the feed rate of roller f, thinning ratio per pass ψ_i, and axial offset a and radial offset b, as reported by Wang et al. [14].

According to Wang et al. [14], for most body-centered cubic (BCC) crystal materials, the range of roller feed rate should be selected as 0.1-1.5 mm/rev; and for low-carbon steel, it should be in the range of 0.2-1.0 mm/rev. Considering both process efficiency and forming quality, different values of roller feed rate are selected as 0.4 mm/rev, 0.6 mm/rev and 0.8 mm/rev in this study. Hayama

Masujiro et al. [15] claimed that in order to obtain the small ovality of spun tubes, the feed rate at the first two roller passes should be large, thus they are set to be 0.8 mm/rev. To ensure the surface quality of the spun tubes, the feed rate of final roller pass should be small, thus the value of 0.4 mm/rev is used. To improve process efficiency, for the roller passes between the first two and final passes, the feed rate is set as 0.6 mm/rev. The previous research shows that when the total thinning ratio ψ_t ($\psi_t = (t_0-t_f)/t_0$, where t_0 is the initial wall thickness of the tubular blank, t_f is the wall thickness of the tubular parts) is greater than 80%, the grain refining effect is at the best. The optimum thinning ratio per pass ψ_i ($\psi_i = (t_{i-1}-t_i)/t_{i-1}$, where t_{i-1} is the wall thickness of the tubular parts after i-1 passes spinning, t_i is the wall thickness of the tubular parts after i passes spinning) for cylindrical blank power spinning is 30%~45%, as reported by Xia et al. [12]. Table 1 summaries the process parameters per pass used in the experimental investigation of the 4 mm thick ASTM 1020 steel tube and the 2 mm thick ASTM A36 steel tube.

Table 1 Process parameters per pass in stagger power spinning.

	Parameters	Pass 1	Pass 2	Pass 3	Pass 4	Pass 5
	f / (mm/rev)	0.8	0.8	0.6	0.6	0.4
ASTM 1020 steel	ψ_i	35%	38%	35%	43%	42%
tube (4 mm)	ψ_t	35%	60%	74%	86%	90%
ASTM A36 steel	ψ_i	35%	38%	43%	-	-
tube (2 mm)	ψ_t	35%	60%	78%	-	-

The axial offset a and radial offset b between rollers are closely related to process efficiency and forming quality of spun part. A higher value of the axial offset may result in the discontinuous material deformation, however, a too small axial offset may result in the poor surface smoothness as reported by Xue et al. [16]. In this study, the axial offset a and radial offset b are calculated by following equations, as reported by Li [17] and Gao et al. [18].

$$\begin{cases} \Delta t_1 + \Delta t_2 + \Delta t_3 = \psi_i \cdot t_0 & (1) \\ \Delta t_1 \geq \Delta t_2 \geq \Delta t_3 & (2) \\ b_{12} = \Delta t_2 & (3) \\ b_{23} = \Delta t_3 & (4) \end{cases}$$

$$\begin{cases} K_1 = t_0 \ln \dfrac{t_0}{t_1}\sqrt{\operatorname{ctg}\alpha_1} & (5) \\ K_2 = t_1 \ln \dfrac{t_1}{t_2}\sqrt{\dfrac{t_0}{t_1}\operatorname{ctg}\alpha_2} & (6) \\ K_3 = t_2 \ln \dfrac{t_2}{t_3}\sqrt{\dfrac{t_0}{t_2}\operatorname{ctg}\alpha_3} & (7) \end{cases}$$

$$\begin{cases} a_{12} = f\dfrac{t_0}{t_1}N & (8) \\ a_{12} \geq \dfrac{f}{3}\dfrac{t_0}{t_1} + \Delta t_2 \operatorname{ctg}\alpha_2 + r_2 \sin\alpha_2 - r_2(1-\cos\alpha_2)\operatorname{ctg}\alpha_2 & (9) \end{cases}$$

$$\begin{cases} a_{23} = f\dfrac{t_0}{t_2}N & (10) \\ a_{23} \geq \dfrac{f}{3}\dfrac{t_0}{t_2} + \Delta t_3 \operatorname{ctg}\alpha_3 + r_3 \sin\alpha_3 - r_3(1-\cos\alpha_3)\operatorname{ctg}\alpha_3 & (11) \end{cases}$$

$$N = m + 1/3 \quad (12)$$

where, Δt_1, Δt_2, Δt_3 is the radial reduction of blank radius after each roller pass, as shown in Fig.1. ψ_i is the thinning ratio of wall thickness per pass; K_1, K_2, K_3 is the variable factor of each roller, which represents the radial force undertaken by roller 1, roller 2 and roller 3 during stagger spinning; a_{12} and a_{23} is the axial offset between roller 1 and roller 2, and roller 2 and roller 3, respectively; b_{12} and b_{23} is the radial offset between roller 1 and roller 2, and roller 2 and roller 3, respectively; f is the feed rate of rollers; t_0 and t_1, t_2, t_3 is the thickness of tubular blank and spun part underneath each roller; α_1, α_2, α_3 is the forming angle of the rollers; r_1, r_2, r_3 is fillet radius of the rollers, as shown in Fig.3; m is a integer.

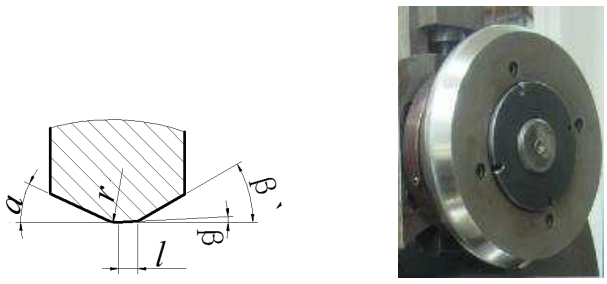

Fig.3. Key dimensions of roller.

As mentioned previously, the thinning ratio of first pass ψ_1=35%, and the thickness of the tubular blank t_0=4 mm are used in this study, thus the total wall thickness reduction under three rollers is 1.4 mm. Therefore, the radial reduction of tubular blank radius can be selected as $\Delta t_1 = \Delta t_2 = 0.5$ mm,

Δt_3= 0.4 mm according to Eqs. (1) and (2). Thus K_1=0.78, K_2=0.84 and K_3=0.73 are determined according to Eqs. (5) - (7), which meet the requirement that the difference among K_1, K_2 and K_3 should be less than 20% to equilibrate the radial force undertaken by each roller, as reported by Li [17]. Therefore, the radial offset b is selected as b_{12}= 0.5 mm and b_{23}=0.4 mm according to Eqs. (3) and (4). Taking f =0.6 mm/rev, the minimum values of a_{12} and N are 2.63 and 3.84 respectively according to Eqs. (8) and (9). Thus m=4 and N=4.33 are determined according to Eq. (12). Finally, the axial offset a_{12} between roller 1 and roller 2 is 2.9 mm according to Eq. (8). Similarly, the axial offset a_{23} between roller 2 and roller 3 is 2.6 mm according to Eq. (10) - (12).

The rotational speed of mandrel has not shown obvious influence on the macro forming quality, as reported by Xia et al. [19]. Therefore, the rotational speed of mandrel is selected according to the machine capacity to be 108 rev/min.

2.3 Experimental equipment and samples

The experiments are carried out on the HGPX-WSM spinning machine, as reported by Xia et al. [9]. The tubular blanks used for the experiment are welded ASTM A36 steel tubes and annealing seamless ASTM 1020 steel tubes, as shown in Fig.4. The dimension of the welded ASTM A36 steel tube is Φ111 mm×2 mm×110 mm, and the seamless ASTM 1020 steel tube is Φ76 mm×4 mm×80 mm.

To provide a stable contact condition between the rollers and blank at the initial spinning stage and to prevent the diameter of tube from expanding at the opening-end after spinning, the blanks are chamfered by 25° in accordance with the forming angle of the rollers. The mechanical properties of ASTM A36 and ASTM 1020 steel are listed in Table 2.

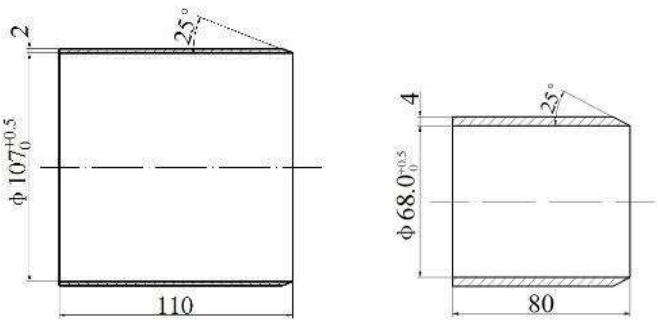

Fig.4. Tubular blanks: (a) Welded ASTM A36 steel tube, (b) Seamless ASTM 1020 steel tube.

Table 2 Mechanical properties of ASTM A36 and ASTM 1020 steel.

Material	Yield stress σ_s /MPa	Tensile stress σ_b /MPa	Hardness /HB	Elongation δ /%
ASTM A36	235	375-500	120	23
ASTM 1020	325	535	150	35

The double-tapered rollers (as shown in Fig.3) are developed to improve the surface smoothness of spun tubes. For thin-walled soft materials, such as low carbon steels and aluminium alloys, the suitable forming angle α is 15°-30°, sleeking angle β is usually 3°-5°, receding angle $\beta`$ is 20°-30°, fillet radius r is 3-10 mm, and polishing belt length l is 3-6 mm, as reported by Wang et al. [14]. Therefore, the key geometric dimensions of rollers are determined as following: forming angle $\alpha$ =25°, sleeking angle $\beta$ =3°, receding angle $\beta`$ =30°, fillet radius r =6 mm, and polishing belt length l = 5 mm.

The dimensional accuracy, mechanical properties and metallographic structures of spun tubes are measured by PX-7 ultrasonic thickness gauge, SHIMADZU AG-X electronic testing machine, HVS -1000S digital hardness tester, JSM6490LV field-emission Scanning Electron Microscopy (SEM), and JEM-2100 Transmission Electron Microscopy (TEM).

2.4 Experimental procedures

The grain size of materials after plastic deformation is closely related to the initial grain size, the degree of deformation and heat treatment conditions, as reported by Mishra [20]. Therefore, two experimental procedures are designed to refine the grains by considering material phase transformation, process optimization and heat treatment, to achieve the purpose of integrated control of forming quality and microstructural evolution for manufacturing tubes using power spinning.

Process Method One - Multi-pass stagger spinning: Firstly, the 5-pass stagger backward spinning is conducted, and the total thinning ratio of the tubular blank is 90%. Secondly, one-way backward spinning without any thinning ratio is carried out repeatedly by keeping the clearance λ between rollers and mandrel exactly equal to the wall thickness of spun tube.

Process Method Two: The process consists of 3-pass spinning followed by a 580 ºC× 0.5 h static recrystallization, 2-pass spinning and a 580 ºC×1 h static recrystallization annealing. The spun tubes after three passes spinning (as shown in Table 1) are annealed at 580 ºC for 0.5 h then air-cooled to acquire the equiaxial grains and to eliminate the residual stresses. Final spinning with 42% thinning ratio is followed by recrystalization annealing to refine the grains to nano/submicron scale homogeneous grains.

3. Results and discussion

3.1 Macro forming quality of spun tubes

Using Process Method One, the spinning process of ASTM A36 steel performed successfully when the total thinning ratio was less than 78%, while cracks occurred at welding region when the total thinning ratio reached 78%, as shown in Fig.5. However, for ASTM 1020 steel, the whole spinning process performed successfully even when the total thinning ratio reached 87%, as shown in Fig.6.

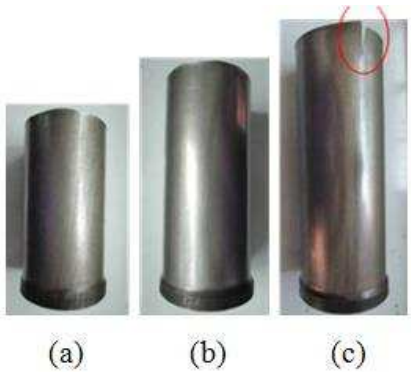

Fig.5. ASTM A36 steel spun tubes under different total thinning ratio using method one: (a) ψ_t=35%, (b) ψ_t=60%, (c) ψ_t=78%.

Fig.6. ASTM 1020 steel spun tubes under 87% total thinning ratio using method one.

Using Process Method Two, the whole spinning process also performed successfully apart from a slight decrease of surface smoothness due to the recrystallization annealing, good surface smoothness and spin-formability of spun tubes were achieved under 87% total thinning ratio, as shown in Fig.7. The wall thickness deviation of spun tubes under 87% thinning ratio using Process Method Two is less than 0.05 mm, as reported by Yang [21].

Results of ASTM 1020 steel spun tubes in Process Method Two will be discussed in details in the following section.

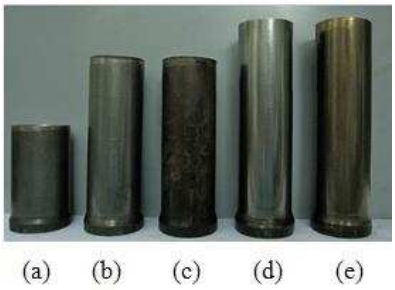

Fig.7. Spun tubes under different thinning ratio of ASTM 1020 steel using method two: (a) ψ_t= 35%, (b) ψ_t= 70%, (c) annealed tube, (d) spun tube (ψ_t= 87%) after annealing, (e) final annealing.

3.2 Microstructural evolution of spun tubes

3.2.1 Microstructure characterization methods

(1) Scanning electron microscopy

The JSM6490LV field-emission SEM is used. The surface smoothness of specimen (10 mm ×5 mm) for optical microscopy observation is 0.1 μm prepared by mechanically polish, and then the specimen is etched by the 4% HNO_3 + 96% $C_2H_4O_2$ solution.

(2) Transmission electron microscopy

The TEM observation is carried out by using a JEM-2100 instrument. The size distribution of the ferrite grains is measured and characterized in terms of the mean linear intercepts from the SEM and bright field TEM images. The TEM samples are produced by the mechanical polishing to the thickness of about 50 μm, followed by the electropolishing based on the MTP-1A double jets instrument in the 4% $HClO_4$ + 96% $C_2H_4O_2$ at -40 ^{o}C and 75 V voltage.

3.2.2 SEM analysis

Fig.8 shows the evolution of pearlitic cementite lamellae based on the SEM during power

spinning and subsequent annealing. Fig.8 (a) shows the initial lamellar pearlitie structure of ASTM 1020 steel tubular blank consisting of the ferrite and cementite plates. Fig.8 (b) and (c) show that as the thinning ratio increases during power spinning, the deformation and the irregular bend of the pearlitic cementite lamellae occur and the lamellae tends to arrange along the direction parallel to the material flow direction. Such phenomenon has also been observed in pearlitic steels during wire draw, as reported by Michael et al. [22] and Toribio et al. [23]. Finally, the cementite is gradually crashed to the granular carbide distributing on ferrite grain boundaries and acting as obstacle to grain boundary migration during annealing, as shown in Fig.8 (d).

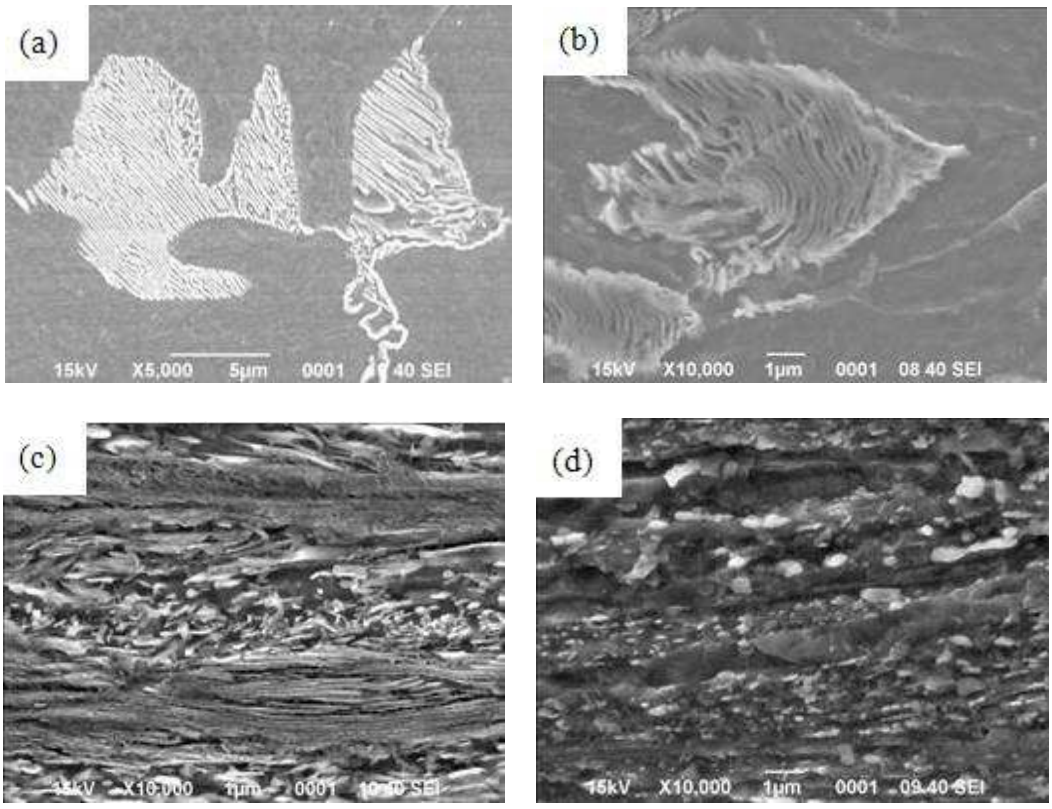

Fig.8. Evolution of pearlitic cementite lamellae based on the SEM during power spinning and subsequence annealing: (a) pearlitic cementite lamellae of ASTM 1020 steel tubular blank, (b) pearlitic cementite lamellae after deformation under ψ_t=60%, (c) pearlitic cementite lamellae after deformation under ψ_t=87%, (d) pearlitic cementite lamellae after 580 ºC annealing for 1 h.

3.2.3 TEM analysis

The microstructure of ASTM 1020 steel is composed of ferrite and cementite phase, and the initial ferritic grain size is 50 μm. Fig.9 shows the two prominent deformation features based on

TEM micrographs during power spinning under 87% thinning ratio. It shows that the brittle and stiff cementite phase is firstly crushed into granule during spinning and then act as an emission source to release a great number of dislocations, as shown in Fig.9 (a), where the plastic deformation is mainly occurred in the ferrite phase. The ferrite phase is elongated along the axial direction and formed the fiber structure with a certain orientation, and a large number of dislocation cells and dislocation tangles are formed inside the interior of the ferrite matrix grains, as shown in Fig.9 (b).

Figure.10 shows the generation of subgrains in the original large grain interior and the evolution of boundary misorientations when the equivalent strain is 2.27 (ψ_t= 87%). It shows that the grain subdivided into the eight small subgrains with various sizes. There are three kinds of boundary morphologies. The first one is the original large grain boundary, the boundary on the right side of subgrains 3, 4, 5, 7, 8. The second one is the boundaries between subgrains 2 and 3, 4 and 5, and 6 and 7, which are clear and show the amount of high density dislocations. The third one is the boundaries between the subgrains 1 and 2, 3 and 4, 5 and 6, 6 and 8, which are not clear and will transform to large-angle grain boundary under further plastic deformation. Moreover, the form of boundaries between grains varies with the increase of the location density inside the subgrains boundaries when the thinning ratio increases, for example, the low-angle boundary will evolve into the high-angle boundary by absorbing dislocations. There are some similarities between the microstructural evolution of materials subjected to power spinning and other SPD processes. All processes initially produce cellular structures with low-angle misorientations inside initial large grains. The misorientation increases with increasing strain, forming high-angle boundaries, the fraction of which increases with increasing strain [24].

Fig. 11 shows the TEM micrographs of the spun tubes after severe power spinning under 87% thinning ratio of wall thickness reduction and subsequence annealing at 580 ^{o}C for 1h heat preservation. Fig.11 (a) shows that the main crystallographic textures are the ultra-fine ferrite grains and globular cementites. The average size of ferrite grains is 500 nm and the fine cementite particles are homogeneously distributed inside the ferrite grains. The dislocation density near grain boundaries is greater than that of the inner grains, and the grain boundaries are faded which indicates that the crystallographic texture is in a nonequilibrium state caused by high internal stresses. The black and white arrows illustrate the dislocation wall and cellular structure caused by

dislocation tanglement (Fig.11 (a)). The ultrafine-grained structures obtained in the present investigation have the typical characteristic of nonequilibrium, which is consistent with those observed in other SPD processes [4, 25, 26].

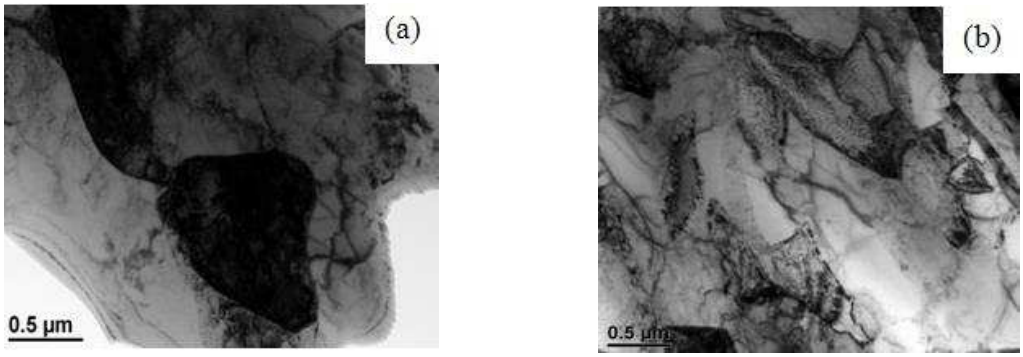

Fig.9. Two prominent deformation features based on the TEM during power spinning (ψ_t=87%): (a) cementite particle as emission source of dislocation, (b) dislocation cells and tangling in ferrite matrix.

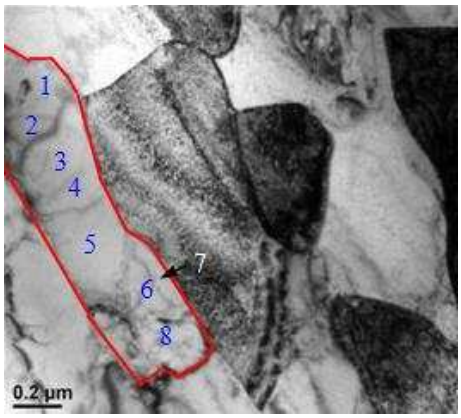

Fig.10. Formation of subgrains based on TEM during power spinning (ψ_t=87%).

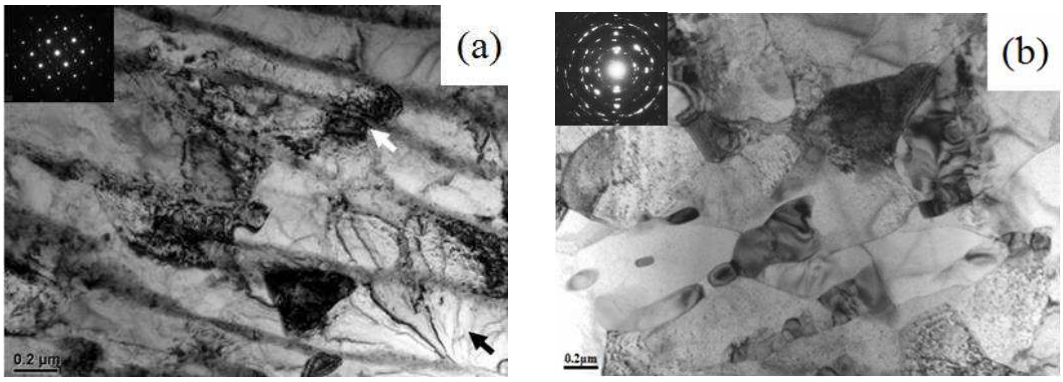

Fig.11.TEM image of spun tube: (a) spun tube under ψ_t=87%, (b) spun tube after annealing at 580 ºC for 1 h.

Although the grain refinement of pure metals and alloys can be achieved by SPD, these ultrafine grains may not be stable at high temperature, in the deformed structured region recrystallization takes place due to high dislocation density, as reported by Minoru [27]. Fig.11 (b) shows that the grain orientations are disappeared and the fine isometric crystals is generated after annealing at 580 ºC for 1 h. The dislocation both on grain boundaries and inner grains decrease greatly and the grain boundaries become more clearly, some globular cementites are homogeneously distributed inside the ferrite grains or on the boundaries. Fig.12 shows the distribution of gain sizes of ferrite of the spun tubes under 87% thinning ratio of wall thickness reduction and subsequence annealed at 580 ºC for 1h heat preservation. It shows that the range of the size of the ferrite grains is mainly concentrated from 0.4 to 1.2 μm, and the average size of ferrite grains is approximately 600 nm.

During the power spinning, the dislocation density is increased with the dislocation gliding, accumulation and tangling, and the boundaries of cellular substructure are formed simultaneously. Similar observations have been reported in ultrafine grain structure of aluminium alloy 7075 manufactured by ultrasonic shot peening, as reported by Wu [28]. During the subsequence annealing, the dislocation inside the interior of dislocation cells is glided to the dislocation walls with the decrease of the storage energy of deformation. The opposite sign dislocations interact with each other on the same slip plane and disappeared, which leads to the decrease of the dislocation density; the subgrain boundaries are formed through the gliding and climbing of the same sign dislocations; the recrystallization nucleation occurs at the area of the high dislocation density, and then the crystal nucleus grows to the equiaxial grain without distortion.

As discussed in the above, the microstructural evolution of ASTM 1020 steel during power spinning could be regarded as the grain subdivision. Firstly, dislocations increase gradually inside grains, the strength of grains is usually considered to be less than that of grain boundaries, to form cellular structure caused by severe plastic deformation. Then cellular structures transform into subgrains under further plastic deformation. Finally, new grains with high-angle grain boundaries are generated.

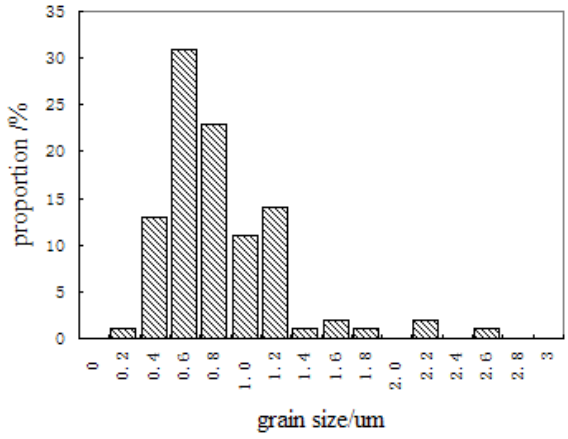

Fig.12. Distribution of ferrite grain sizes.

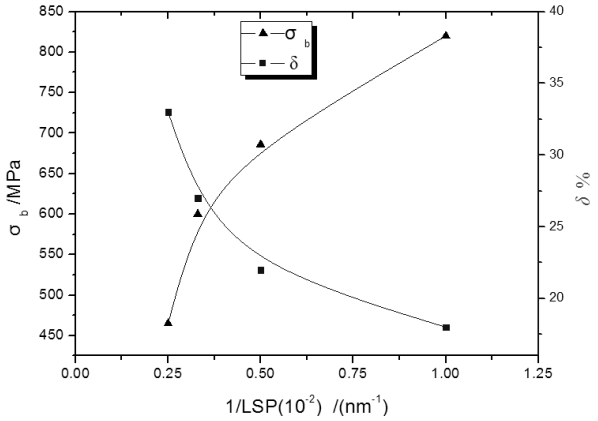

Fig.13. Effect of LSP on mechanical properties of spun tubes.

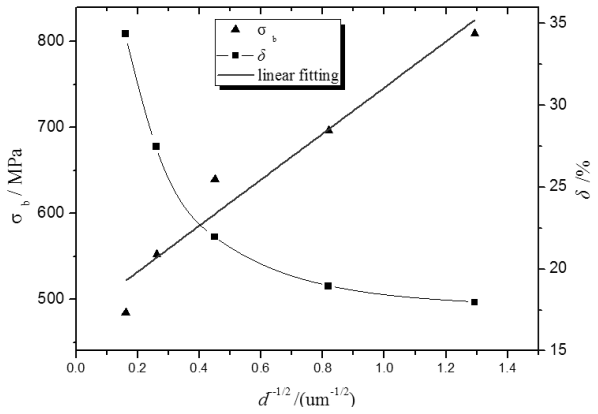

Fig.14. Effect of grain sizes on mechanical properties of spun tubes.

3.3 Variation of mechanical properties of spun tubes

3.3.1 Influence of LSP on mechanical properties

The measurement of LSP (layer spacing of pearlite) is carried out by using the SEM. The mechanical properties of tensile stress and elongation shown in Fig. 13 and 14 are measured

through the uniaxial tension test after each spinning pass without annealing. The value of LSP decreases from 400 nm (tubular blank) to 100 nm (spun tube under ψ_t=87%), the corresponding tensile strength σ_b increases from 465 MPa to 820 MPa and the elongation δ decreases approximately 17%, as shown in Fig.13.

Fig.13 shows that the LSP decreases greatly as the thinning ratio of wall thickness reduction increases during power spinning. Accordingly, the tensile strength σ_b of spun tubes is proportional to the reciprocal of LSP. However, the elongation δ is inversely proportional to the reciprocal of LSP.

3.3.2 Influence of grain size on mechanical properties

Fig. 14 illustrates the relationship between tensile strength, elongation and grain size. The tensile strength, elongation and grain size are measured after each spinning pass without annealing. It shows that the tensile strength σ_b of spun tubes increases linearly with the grain sizes decreases, and its linear correlation coefficients k = 0.26 MPa·$\mu m^{1/2}$. The tensile strength of the spun parts is in a good conformity with Hall-Petch relationship, even for submicron grain structures, which is similar to that of the AA1100 aluminum sheet formed by ARB, as reported by Pirgazi [29]. However, the variation of elongation δ is a more complicated. With grain sizes decreases, firstly, due to the work hardening, the elongation drops sharply; and then decreases slowly when the grain size reaches sub-micron or nano scale because of the combined effect of work hardening and fine-grain strengthening.

4. Conclusions

A new method of manufacturing tubes with nano/ultrafine grain structure by combining spinning and heat treatment technologies has been proposed. Two methods of the stagger spinning process are developed and corresponding experiments are carried out. The following conclusions may be drawn:

(1) A good surface smoothness and an improved spin-formability of spun parts can be obtained by the process method combining of 3-pass spinning followed by a 580 ºC× 0.5 h static recrystallization and 2-pass spinning with a 580 ºC×1 h static recrystallization annealing under the severe thinning ratio of wall thickness reduction.

(2) After the multi-pass stagger spinning, the ferrites of the original isometric crystals is stretched along axial direction and the cementite is crashed to the granular carbide gradually with the thinning ratio of wall thickness reduction increases, resulting the fiber structures with a certain orientation being formed.

(3) The irregular bend of the pearlitic cementite lamellae occurs, and the subgrain boundaries and grain boundaries are generated from the dislocation walls through the dislocation accumulation and tangling when the thinning ratio of wall thickness reduction increases during power spinning.

(4) The ferritic grains with the average initial size of 50 μm are refined to 500 nm after stagger spinning under the 87% thinning ratio of wall thickness reduction. The small equiaxial ferritic grains are generated at the position of severe lattice distortion in the spun tubes through re-nucleation and grain growth by subsequence recrystallization annealing at 580 ºC for 1 hour heat preservation, the average size of the equiaxial grain is approximately 600 nm.

(5) The layer spacing of pearlite (LSP) decreases with the thinning ratio of wall thickness reduction increases during power spinning. The tensile strength σ_b of spun tubes is found to be proportional to the reciprocal of LSP, and the elongation δ is inversely proportional to the reciprocal of LSP.

(6) A large strain gradient appears in the cross section of spun tubes by means of power spinning. The further study should focus on effects of spinning process methods on the distribution of grain sizes along the cross-section of the spun tubes.

Acknowledgments

This project was financially supported by National Natural Science Foundation of China (51075153), Natural Science Foundation of Guangdong Province (10151040301000000) and Key Laboratory of Precision Equipment and Manufacturing Technology of Guangdong Province (PEMT1202).

References

[1] Terry, R., McNelley, Alexandre, P. Z., Srinivasan, S., et al. Application of EBSD Methods to Severe Plastic Deformation (SPD) and Related Processing Methods. Electron Backscatter

Diffraction in Materials Science 2009:277-289.

[2] Valiev, R. Z. Developing SPD methods for processing bulk nanostructured materials with enhanced properties. Mets. and Mater. Int 2001;7(5):413-420.

[3] Stoica, G. M. Equal-Channel-Angular Processing (ECAP) of Materials: Experiment and Theory. Dissertation of the University of Tennessee, Knoxville 2007.

[4] Jiang, H. G., Zhu, Y. T., Igor V. Alexandrov, et al. Microstructural evolution, microhardness and thermal stability of HPT-processed Cu. Mats. Sci. and Eng 2000; 290:128-138.

[5] Salimi, S., Izadi, H., Gerlich, A. P. Fabrication of an aluminum carbon nanotube metal matrix composite by accumulative roll-bonding. J. Mater. Sci 2011;46:409-415.

[6] Yang, X. Y., Sun, Z. Y., Miura, H., et al. Grain size and texture changes of magnesium alloy AZ31 during multi-directional forging. Trans. Nonferrous Met. Soc. China 2008;18: 200-204.

[7] Wang, L., Long, H. Investigation of Material Deformation in Multi-Pass Conventional Spinning. Materials and Design 2010;32:2891-2899.

[8] Wong, C. C., Dean, T. A., Lin, J. A review of spinning, shear forming and flow forming processes. J. Mater. Process. Technol 2004;153-154:60-66.

[9] Xia, Q. X., Cheng, X. Q., Ruan, F., et al. Finite Element Simulation and Experimental investigation on the Forming Forces of 3D Non-axisymmetrical tubes spinning. Int. J. Mech. Sci 2006a; 48 (7):726-735.

[10] Hamid, R., Molladavoudi & Faramarz Djavanroodi. Experimental study of thickness reduction effects on mechanical properties and spinning accuracy of aluminum 7075-O, during flow forming. Int. J. Adv. Manuf. Technol 2011;52:949-957.

[11] Xu, W. C., Shan, D. B., Wang, Z. L., et al. Effect of spinning deformation on microstructure evolution and mechanical property of TA15 titanium alloy. Trans. Nonferrous Met. SOC. China 2007;17:1205-1211.

[12] Xia, Q. X., Zhang, P., Yang, B. J., et al. Orthogonal experimental study on forming process parameters of tube stagger spinning. Forging & Stamping Technology 2012a ;37(6):45-49 (In Chinese).

[13] Cheng, X. Q., Sun, L. Y., Xia, Q. X. Processing Parameters Optimization for Stagger Spinning of Trapezoidal Inner Gear. Adv. Mats. Research 2011;189-193:2754-2758.

[14] Wang, C. H., Liu, K. Z. Spinning technology. China Machine Press, Beijing, 1986:441-467 (In

Chinese).

[15] Hayama, M. Spinning Technology. Cheng, J. Z. Trans. China Machine Press, Beijing,1984:68-70 (In Chinese).

[16] Xue, K. M., Lu, Y., Zhao, X. M. A study of the rational matching relationships amongst technical parameters in stagger spinning. J. Mater. Process. Technol 1997;69:167-171.

[17] Li, M. S., 2011. Review of cylindrical part stagger spinning technology. In: Proceedings of 12th national annual conference of spinning technology. pp. 6-10 (In Chinese).

[18] Gao, S, Qiu, M.X. Accurate calculation of axial offset during stagger spinning. Forging & Stamping Technology 1994, 5: 46-49.

[19] Xia, Q. X., Susumu, S. S., Kotera, H., et al. A study of the one-path deep drawing spinning of cups. J. Mater. Process. Technol 2005a; 159(3):397-400.

[20] Mishra, A. Microstructural evolution in ultra-fine grained copper processed by severe plastic deformation. Dissertation of University of California, San Diego.2007.

[21] Yang, B. J., Xia, Q.X., CHENG, X.Q. Investigation on fabrication of ultrafine-grain tubular part through power spinning. Journal of Functional Materials2013; Supplement 45: 266-269.

[22] Michael Zelin. Microstructure evolution in pearlitic steels during wire drawing. Acta Materialia, 2002, 50: 4431-4447.

[23] J. Toribio, E. Ovejero. Microstructure evolution in a pearlitic steel subjected to progressive plastic deformation. Materials science and engineering A, 1997, 234-236: 579-582.

[24] Honggang Jiang, Y. Theodore Zhu, Darryl P. Butt. Microstructural evolution, microhardness and thermal stability of HPT-processed Cu. Materials science and engineering A, 2000, 290: 128-138.

[25] Minoru Umemoto. Nanocrystallization of steels by severe plastic deformation. Materials Transaction, 2003, 44(10): 1900-1911.

[26] X. Sauvage, G. Wilde, S. V. Divinski, et al. Grain boundaries in ultrafine grained materials processed by severe plastic deformation and related phenomena. Materials science and engineering A, 2012, 540: 1-12.

[27] Minoru Furukawa, Zenji Horita, Minoru Nemoto. The use of severe plastic deformation for microstructural control. Materials science and engineering A, 2002, 324: 82-89.

[28] X. Wu, N. Tao, Y. Hong, et al. Microstructure and evolution of mechanically-induced ultrafine

grain in surface layer of AL-alloy subjected to USSP. Acta Materialia 50(2002) 2075-2084.

[29] H. Pirgazi, A. Akbarzadeh, R. Petrov, et al. Microstructure evolution and mechanical properties of AA1100 aluminum sheet processed by accumulative roll bonding. Materials science and engineering A, 2008, 497: 132-138.